FE-2341-5
Distribution Categories UC-90g and 93

A HIGH MAGNETIC FIELD MHD GENERATOR PROGRAM

Quarterly Report for the

Period October, 1977 - December 1977

Contract No. EX 76-C-01-2341

PREPARED FOR
THE UNITED STATES DEPARTMENT OF ENERGY

Submitted by

Profs. R. H. Eustis, C. H. Kruger and M. Mitchner,
Adjunct Prof. S. A. Self, and Dr. J. K. Koester

March, 1978

High Temperature Gasdynamics Laboratory
Department of Mechanical Engineering
Stanford University

Foreword

Much of the work on this program is carried out by student Research Assistants and High Temperature Gasdynamics Laboratory staff members in addition to the Principal Investigators. The additional persons involved in a major way with the work reported here are

Dr. Takashi Nakamura
Mr. John P. Barton
Mr. Bradford Bennett
Mr. Kent James
Mr. Marion Jenkins
Mr. Ralph Kowalik

Table of Contents

List of Tables

List of Figures

List of Figures

ABSTRACT

Predictions were made for the results anticipated from an experiment scheduled for April which will investigate fluctuations of thermodynamic and electrical properties as a function of generator configuration and operating conditions. Further work on the laser fluorescence technique has shown it to be promising for the non-obtrusive spatial resolution of gas temperature. Reduction of data from an earlier electrode boundary layer experiment resulted in temperature profiles which showed the effect of Joule heating. Measurements also showed the electron number density near the electrode to be out of equilibrium due to finite electron recombination rates and to Joule heating. Thermal tests continued with the 6 tesla disk generator to determine the most favorable peg size and attachment technique to handle the large thermal load in the disk channel. The major design decisions for the 6 tesla linear generator have been made.

1.0 OBJECTIVE AND SCOPE OF WORK

The objective of the program is to investigate the high magnetic field effects in MHD channels which will influence the design of large scale generators. The work includes the study at high fields of 1) plasma nonuniformities and instabilities and 2) boundary layer and Hall field phenomena. In addition a third activity is centered on the existing Stanford 6 tesla magnet where small scale linear and disk channels are investigated.

2.0 SUMMARY OF PROGRESS TO DATE

The tasks of the contract statement of work have been grouped into three Work Areas as shown in Table 1, Milestones for MHD Research at High Magnetic Fields. The Work Areas which are keyed to the program objectives are

I Plasma Nonuniformities and Instabilities

II Boundary Layer and Hall Field Phenomena

III Six Tesla Magnet Investigations

In Work Area I plans are being made for a series of experiments to measure fluctuations of thermodynamic and electrical properties as a function of electrode configuration and operating parameters. Further measurements of temperature have been made with the laser fluorescence technique and compared to line reversal measurements.

For the tests of fluctuations, predictions have been made of the relative rms pressure amplitudes and the relative phase angles for a number of operating conditions and configurations of the M-2 MHD channel. The relative phase angles between two experimental measurements as a function of frequency can be found by using the coherency function.

Further work with the laser fluorescence temperature measuring technique described in the last Quarterly Report appears to confirm the exponential temperature sensitivity of the fluorescence signal. Comparisons have been made on the bench set-up with line reversal measurements which average temperature over the line of sight. The agreement was not wholly satisfactory and further comparisons are being made. Comparison between a point measurement and a line-of-sight measurement requires adjustment to account for nonuniform conditions in the line of sight. The uncertainty in these adjustments can be reduced for a long, uniform flame and the set up is being modified to provide such a measuring path.

In Work Area II further reduction of data obtained during an electrode boundary layer experiment was undertaken. Measurements of gas temperature profiles were compared with theoretical predictions based on smooth wall turbulence theory. The discrepancy is thought to be due to wall roughness or a problem with the boundary layer wake model and improvements are being made. Also measured electron density profiles were compared with computed

profiles for cases with and without current. Non-equilibrium effects were noted for both cases due to Joule heating or due to finite recombination kinetics.

In Work Area III, progress was made in the disk generator construction technique and in the linear generator design. A number of experiments were made to determine the optimum size of the MgO pegs for the anticipated heat fluxes and brazing and soldering attachments were evaluated. A technique was evolved which will be used on the experiments planned for early April. Studies continued of the boundary layer in a radial flow disk generator. Design decisions were made for the linear 6 tesla MHD channel and engineering calculations to support the detailed design were undertaken. Long lead time items are being identified.

The status of the work is summarized in the program milestone chart, Figure 1.

Table 1

Milestones for MHD Research at High Magnetic Fields

WORK AREA I - Plasma Nonuniformities and Instabilities

Task 1 Plasma nonuniformity study

- 1.1 Initiate development of pressure fluctuation diagnostics
- 1.2 Test of diagnostics in cold channel
- 1.3 Test of diagnostics of M-2 channel
- 1.4 Test of diagnostics in Super M-8 channel

Task 2 Development of temperature fluctuation diagnostics

- 2.1 Initiate bench development of rapid line reversal method
- 2.2 Apply rapid line reversal method to open burner
- 2.3 Apply rapid line reversal method to M-8 channel
- 2.4 Bench development of laser system for spatial resolution
- 2.5 Apply laser system to open burner
- 2.6 Apply laser system to M-8 channel

Task 3 Instabilities

- 3.1 Tests of fluctuation in cold channel (see 1.2)
- 3.2 Initiate test with normal operating conditions in M-2
- 3.3 Initiate test with introduced disturbances in M-2
- 3.4 Begin tests in Super M-8

WORK AREA II - Boundary Layer and Hall Field Phenomena

Task 4 Boundary layer study

- 4.1a Develop LDV techniques
- 4.1b Develop line intensity techniques
- 4.1c Develop line reversal techniques
- 4.1 Initiate development of technique for remote channel operation
- 4.2 Develop access in mock-up of Super M-8 channel
- 4.3 Test of electrode boundary layer in Super M-8 channel
- 4.4 Extend theory to large MHD channels
- 4.5 Complete fabrication of M-8 channel

Task 5 Turbulence damping study

- 5.1 Measurement of turbulence intensity (part of test listed in 4.3)

Table 1 (Continued)

Milestones for MHD Research at High Magnetic Fields

Task 6 Hall field limitation study

- 6.1 Initiate electrode development for Super M-8 channel
- 6.2 Apply field test in Super M-8 channel outside of magnet

Task 7 Electrode configuration study

- 7.1 Electrode development in channel mock-up
- 7.2 Preliminary test of electrode in M-2 channel
- 7.3 Test in Super M-8 channel

Task 8 Current concentration

- 8.1 Initiate development of segmented electrode
- 8.2 Test segmented electrode in M-2 channel
- 8.3 Test segmented electrode in Super M-8 channel

WORK AREA III - Six Tesla Magnet Investigations

Task 9 Disk generator program

- 9.1a Complete construction of disk generator
- 9.1b Complete construction of disk generator exhaust system
- 9.2 Thermal checkout of disk system
- 9.3 Test in 6 tesla magnet

Task 10 Linear 6 tesla channel

- 10.1 Complete design of linear channel for 6 tesla magnet
- 10.2 Complete construction of linear channel
- 10.3 Thermal test outside of magnet
- 10.4 Experiment in 6 tesla magnet with clean fuel
- 10.5 Test in 6 tesla magnet with coal combustion

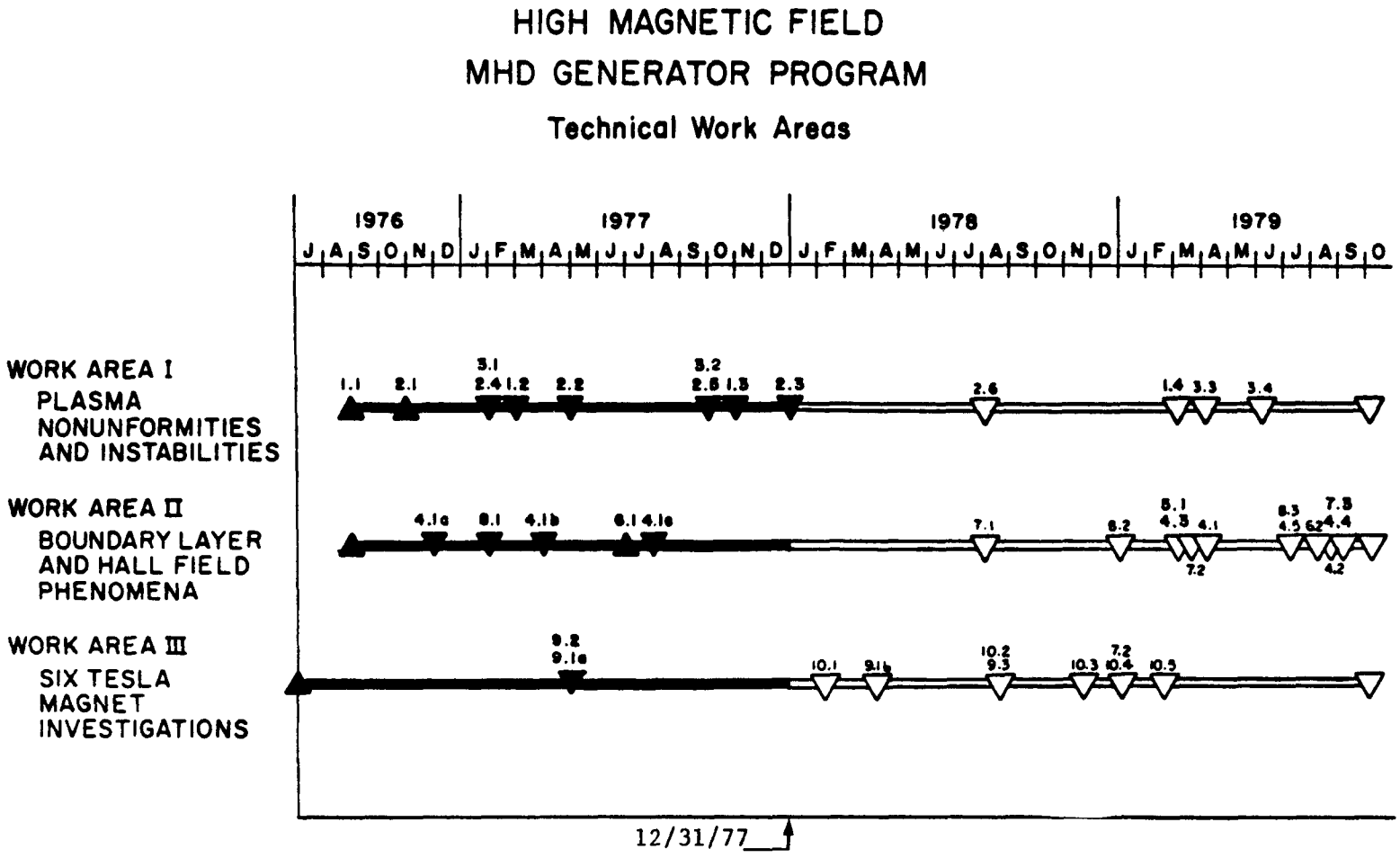

Figure 1. Program Milestone Chart.

3.0 DESCRIPTION OF TECHNICAL PROGRESS

3.1 Work Area I - Plasma Nonuniformities and Instabilities

3.1.1 Plasma Instability Investigations.

Preparations are underway for a further series of experiments utilizing Stanford's M-2 test facility, in which inherent fluctuations of thermodynamic and electrical properties will be measured as a function of the generator electrode configuration and operating parameters. Past results have indicated that a significant increase in low frequency pressure oscillations can occur within a Faraday generator, when operating under high current densities and applied magnetic fields. A new theory in which the generator is treated as a combustor-excited three-wave resonator duct yields results which are in accord with the past experimental measurements. The purposes of the planned experiment are: a) to check the reproducibility of the data obtained in previous experiments, b) to expand the range of conditions for which measurements were taken and, c) to obtain additional results that can be compared with the predictions of the theory. The experiment is planned for March.

The experimental arrangement and procedure will be similar to those of the previous experiment with several refinements. Fluctuations in plasma pressure will be measured using the special pressure probes designed for this purpose. Pressure probes will be located on the combustor plenum wall and at three channel locations along the flow direction. Voltage fluctuation measurements will be made both between the electrodes and between internal voltage pins. Measurements are to be recorded on a multitrack analog tape recorder for post-test statistical analysis. New hardware development will provide expanded experimental capability:

1. Additional external batteries. The external battery supply is being expanded from an available 120 volts per electrode pair to 240 volts per electrode pair. The augmentation of generator voltage is needed to balance near electrode losses and thus provide a better model of an ideal generator. The larger available battery supply will allow higher attainable current densities.

2. New ballast resistors. The values of the external ballast resistors are being changed to provide more flexibility in choosing external loading factors.

3. Analog tape recorder. A new analog tape recorder will provide the accurate simultaneous recording of up to fourteen signals.

4. Current transient measurement. A new set of high common mode rejection differential amplifiers will allow the accurate measurement of current fluctuations.

Both previous experimental work and calculations have shown that the MHD effect on inherent transients is increased as the interaction parameter

$$S \equiv \frac{\sigma B^2 L}{\rho u}$$

gets larger. Calculated values of the interaction parameter for the M-2 facility are shown in Figure 2 as a function of total mass flow rate and the amount of nitrogen addition. The approximate Mach number calculated as a function of mass flow rate is given in Figure 3. It can be seen that the interaction parameter is greatest at low mass flow rates (i.e. small u) with minimal nitrogen addition (i.e. large σ).

The theory which has been developed to describe the observed MHD fluctuations provides a prediction, for a specified excitation frequency, of the relative amplitude and phase angle of the oscillation in each thermodynamic and electrical variable as a function of position along the channel. Through the use of statistical techniques the experimental data can be analyzed to provide a check on the theoretical predictions. Examples of theoretical results are shown in Figures 4 and 5. The amplitude of a signal as a function of frequency, as illustrated in Figure 3, can be found using the spectral density function. The relative phase angle between two experimental measurements as a function of frequency, as illustrated in Figure 4, can be found using the coherency function. Other statistical routines such as the cross correlation function and the probability distribution are also available for analysis of experimental data.

The upcoming series of experiments will be used to obtain additional data and to test our present level of understanding of fluctuation phenomena in MHD generators. Further work will include calculation of the importance of this effect for full-scale central station generators and investigation of possible methods that may be used for the control of fluctuation levels.

3.1.2 Plasma Nonuniformity Studies.

Work has continued on the development of the laser fluorescence diagnostic which will ultimately be used to measure electrical conductivity fluctuation intensities and two-point correlations in an MHD generator. Additional experiments have been conducted with the basic apparatus that was described in the last Quarterly Report. These experiments compared the relative magnitudes of fluorescence signals from two flames with different temperatures. Temperatures in the fluorescing volumes of the flames were obtained from a four step process. First, a relative intensity profile was obtained by measuring the fluorescence signal as the flame was translated perpendicular to the laser beam. This symmetric profile was subsequently converted into a relative temperature profile assuming that the signal was proportional to $\exp(-h\nu_{01}/kT)$, the dominant factor in the rate-equation description of the fluorescence processes. Line-of-sight temperatures were then measured using line reversal methods, and, finally, center-line temperatures were obtained from the experimental reversal temperature by use of a numerical solution of the equation of radiative transfer and the measured relative temperature profiles. Typical results are shown in Fig. 6.

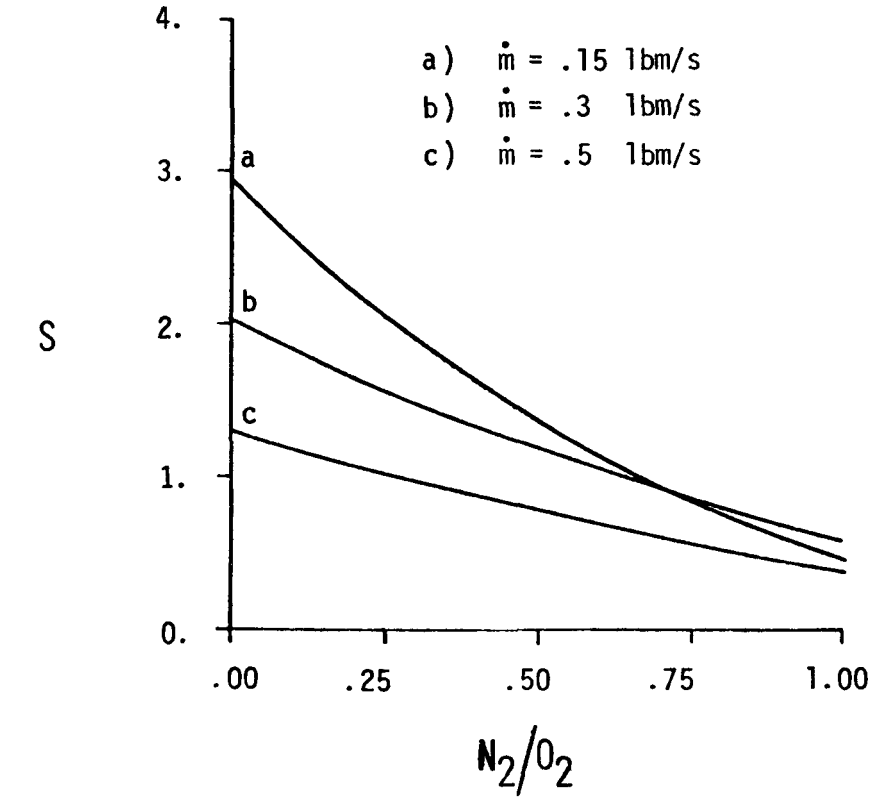

Figure 2. The interaction parameter as a function of total mass flow rate and amount of nitrogen addition as calculated for the M-2 facility. Applied magnetic field B = 2.6 T.

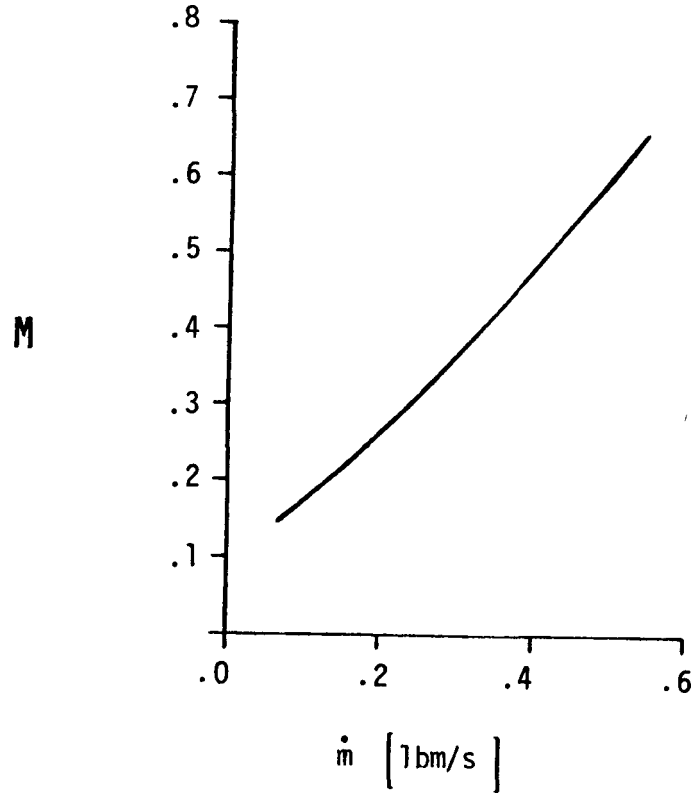

Figure 3. Approximate Mach number as a function of total mass flow rate for the M-2 facility.

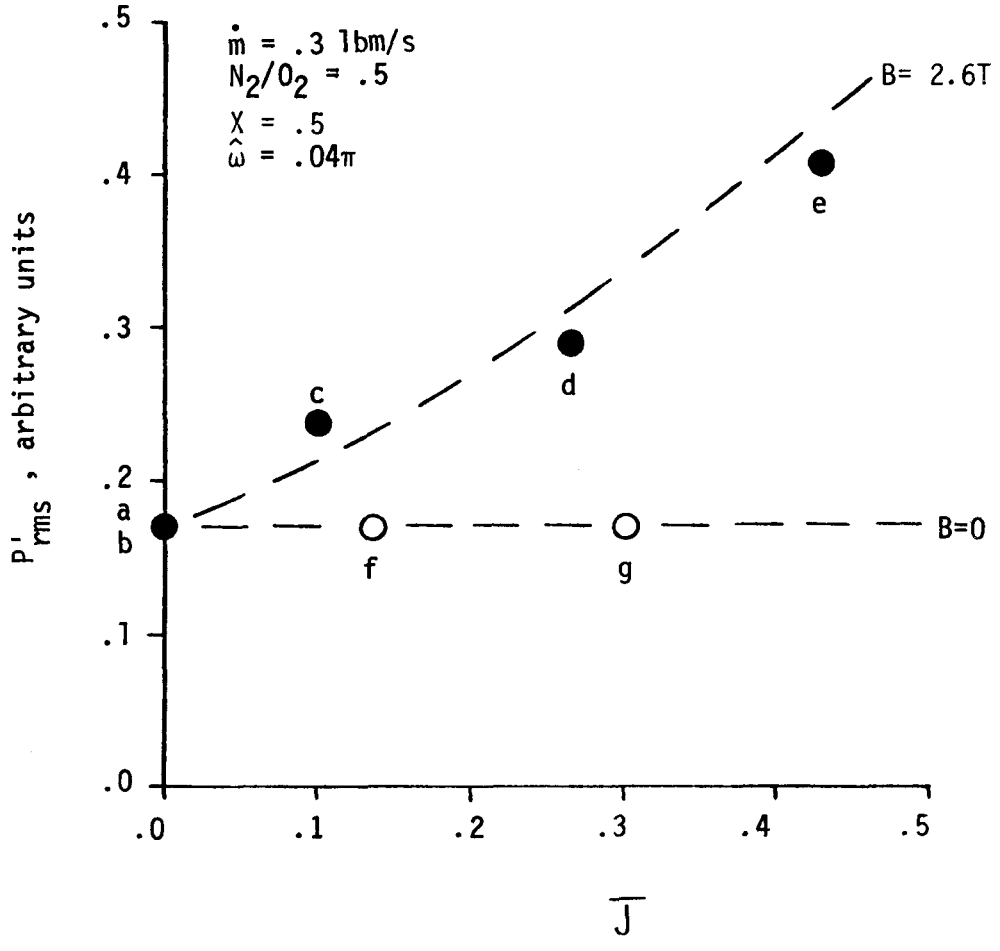

Figure 4. Theoretical relative rms pressure amplitudes for an excitation frequency of 40 Hz as a function of dimensionless current density for the M-2 generator in the Faraday configuration.

Calculations are for x = L/2 and are for the following conditions:

a) open circuit, no applied magnetic field, no applied batteries,
b) open circuit, applied magnetic field, no applied batteries,
c) short circuit, applied magnetic field, no applied batteries,
d) short circuit, applied magnetic field, applied batteries = 120V,
e) short circuit, applied magnetic field, applied batteries = 240V,
f) short circuit, no applied magnetic field, applied batteries = 120V,
g) short circuit, no applied magnetic field, applied batteries = 240V,

$\overline{J} \equiv J/\sigma aB$ $\hat{\omega} = \omega L/a$

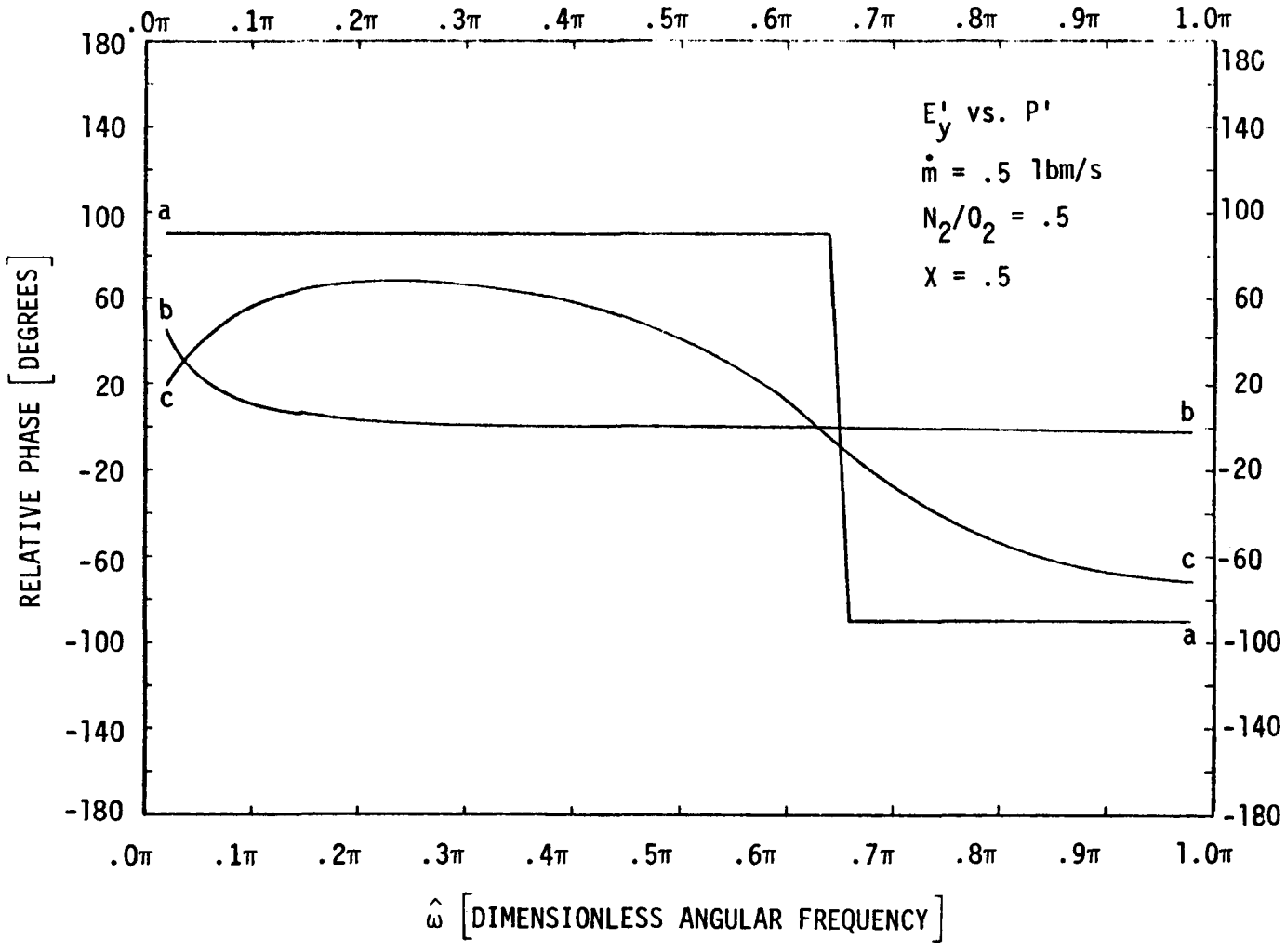

Figure 5. Theoretical phase angle of the transverse electric field relative to pressure for the M-2 generator in the Faraday configuration for the following conditions: a) open circuit, applied magnetic field = 2.6T, no applied batteries, b) short circuit, no applied magnetic field, applied batteries = 120V, c) short circuit, applied magnetic field = 2.6T, no applied batteries.

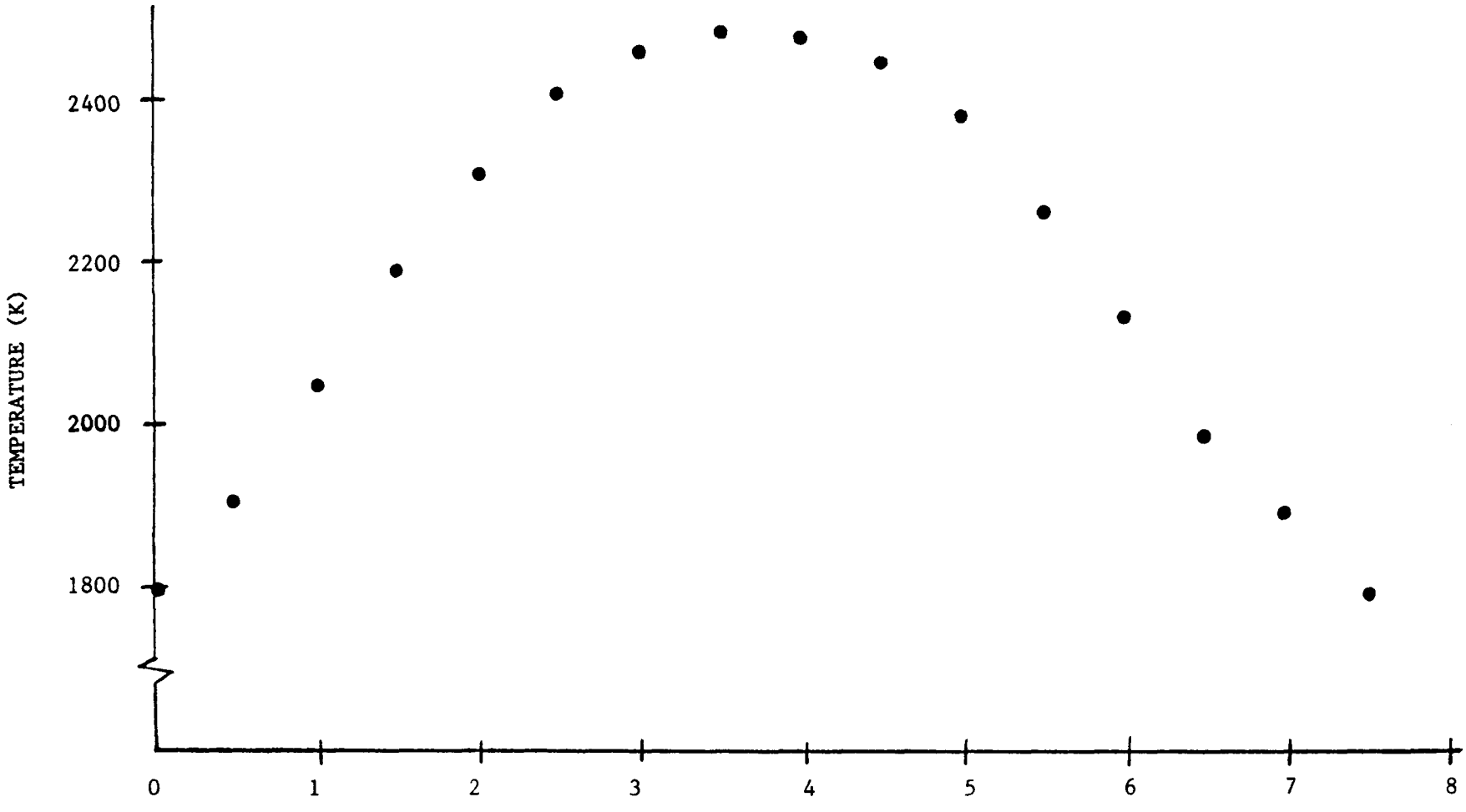

Figure 6. Relative location in flame (MM).

Results of these experiments apparently confirmed the exponential temperature sensitivity of the fluorescence signal; however, the uncertainties in the measurements precluded detailed comparison of the fluorescence theory with experimental data. In particular, the temperature profiles across the narrow dimension of the Perkin-Elmer slot burner were not very flat. This condition reduced our confidence in the interpretation of the line-reversal measurements since there were significant differences between the line-reversal and fluorescing volume temperatures. Also, flame temperatures were varied by changing the equivalence ratio of the mixture input to the burner. The two flames, consequently, had different compositions which may have altered fluorescence signals through quenching as well as temperature factors.

To overcome these shortcomings, additional experiments with the Perkin-Elmer burner are planned and are currently being set up. These experiments will use line-reversal and relative fluorescence intensity data from the wide dimension of the flame. The expected flatter temperature profile should minimize the nonuniformity correction to the measured line-reversal temperatures and thus increase the confidence in the interpretation of the results. Flame temperatures and compositions will be altered by varying both the equivalence ratio and the diluent fraction (extra nitrogen) input to the burner. Results from these experiments should provide data suitable for detailed comparisons of theory and experiment as well as information on composition and quenching uncertainties in laser fluorescence measurements.

In summary, recent experiments have demonstrated the strong temperature sensitivity of the laser fluorescence diagnostic. Currently planned experiments should test the basic theory of the processes involved in the diagnostic and provide information on the expected accuracy of the measurement technique. Future work will concern the additional problems that will be encountered when fluctuation measurements are considered.

3.2 Work Area II - Boundary Layer and Hall Field Phenomena

3.2.1 Electrode Wall Boundary Layer.

Data reduction and theoretical modelling of the results from the applied field boundary layer experiment of summer 1977 have continued. Figure 7 shows results for the temperature profile in the boundary layer, along with a theoretical prediction using smooth wall turbulence theory. A discrepancy between the measurements and theory is noted. This discrepancy is thought to be the result of wall roughness, or a problem with the boundary layer wake model. Theoretical models for including the effects of wall roughness are presently being investigated, and modelling improvements in the wake model parameters are being attempted.

Figure 8 shows measurements of electron number density near the wall for a no-current condition, based on the emission from two different potassium energy states, along with the expected equillibrium number density calculated from the measured temperature profile. The electron number density has been corrected for undertainties in the fundamental constants used in the data reduction by matching the measured electron number density in the channel

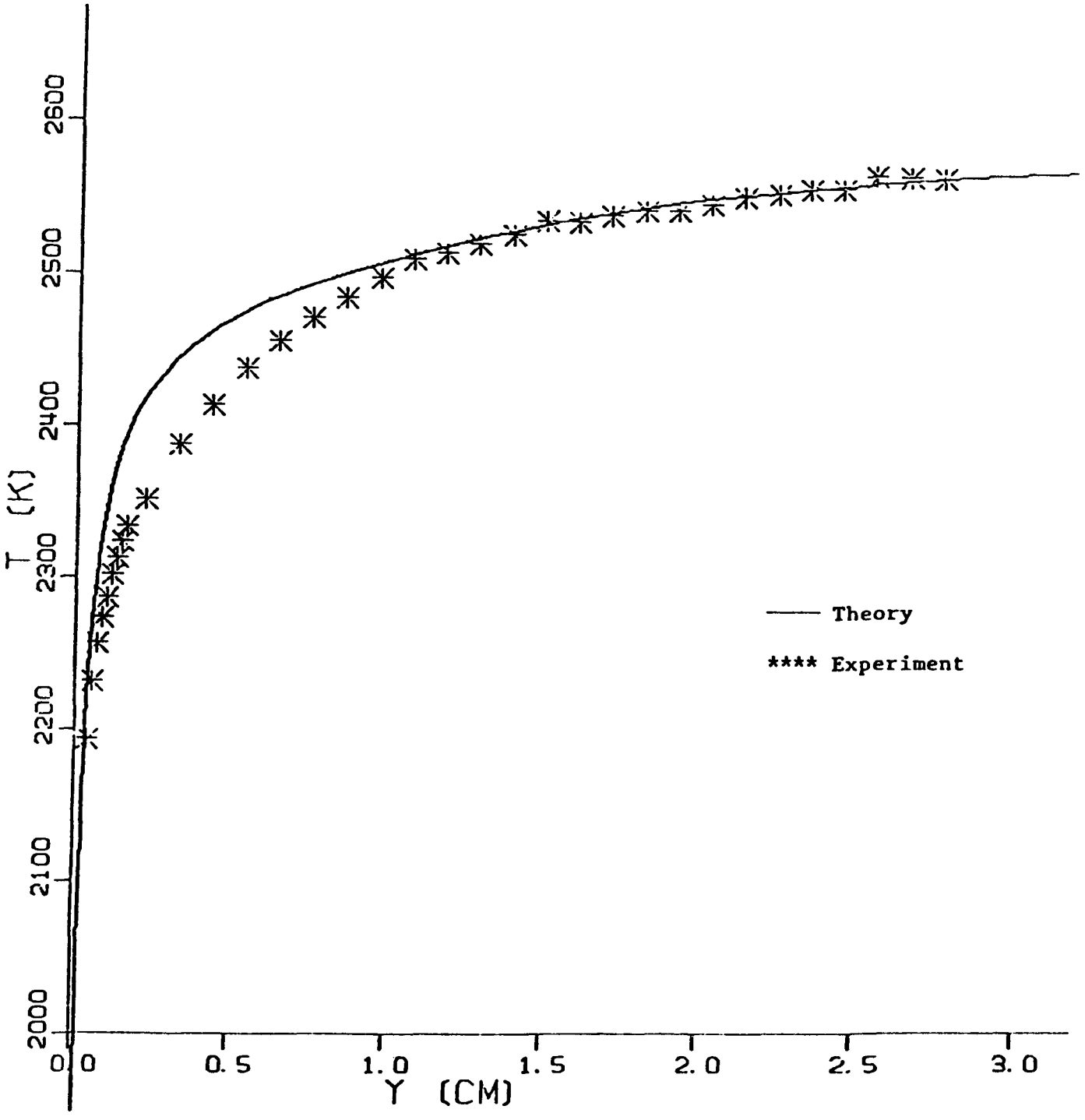

Figure 7. Comparison of Temperature Data to Predictions

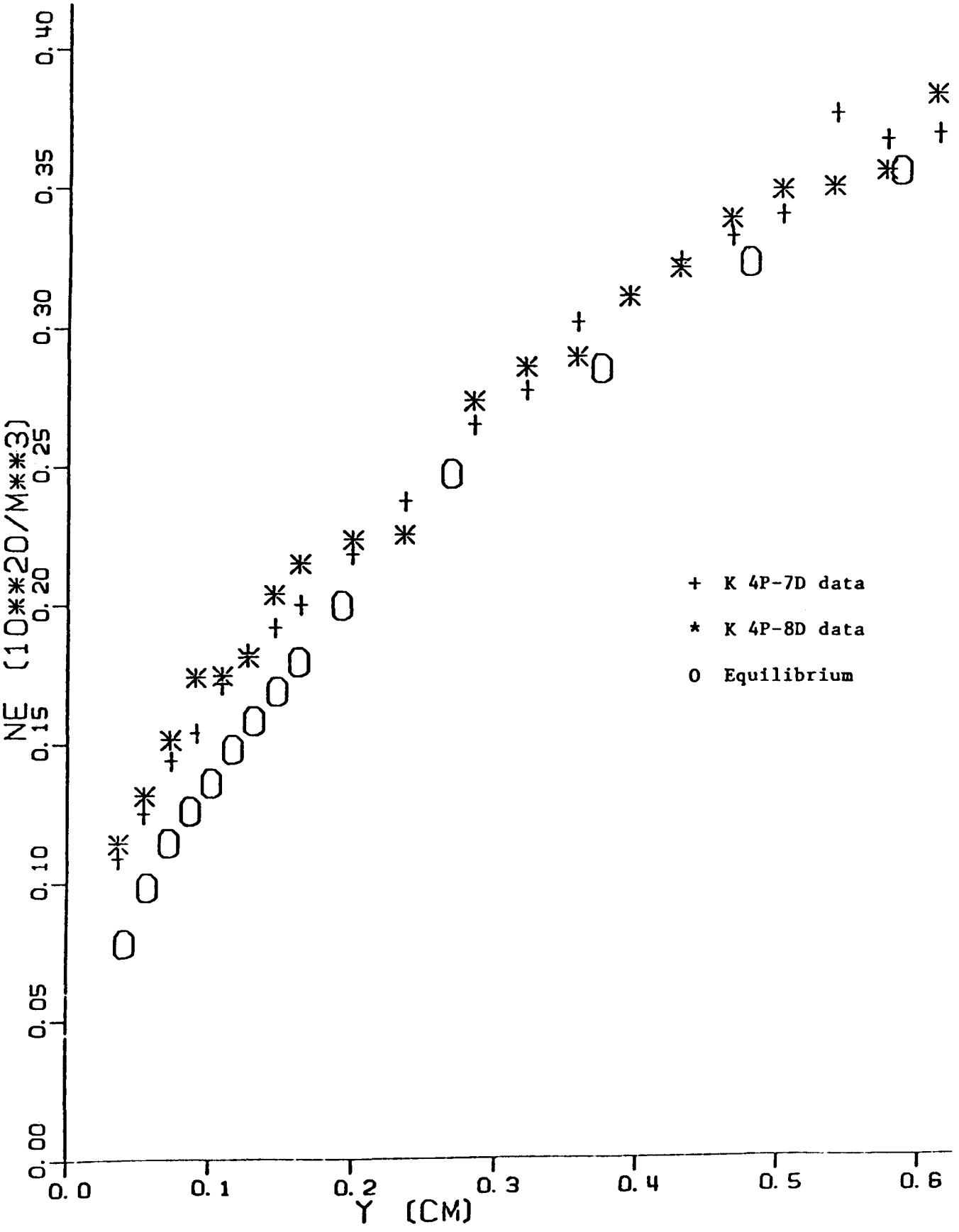

Figure 8. Electron Number Density Data Near the Electrode

centerline, where the electron number density should be in equilibrium, to the equilibrium value based on the measured temperature profile. Very near the wall, non-equilibrium is observed due to the effects of finite rate recombination kinetics. Modelling of the electron number density results will be performed subsequent to the temperature data modelling.

Figure 9 is a plot of electron number density, again corrected by using the temperature profile, for a condition with a very high local current density. The boundary layer was not scanned as long during the runs with high local current density, thus the data is not as clean as the data of Figure 8. Also plotted in Figure 9 is a number density profile for a condition of no current. The very high current density profile has a region near the wall where the electron number density is relatively flat. Although more interpretation of the data is needed, it is possible that a current constriction is occurring in the near electrode region, giving rise to the region of constant electron number density as the constriction elevates the local number density. Figure 10 shows data for anode voltage drops for a series of runs similar to the conditions of Figure 9. As the current density increases, a flattening occurs in the value of the anode voltage drop. This also seems to indicate that a current constriction is occurring in the near electrode region.

The data from the applied field electrode boundary experiment is still being interpreted, so all results presented here should be considered preliminary. Further results will be presented at the 17th EAM Symposium.

3.3 Work Area III - Six Tesla Magnet Investigations

3.3.1 Disk Generator Program.

Efforts were directed to improve the ceramics structure of the disk generator insulator plate. The MgO ceramic insulators of different structures and various sizes were tested. The results indicated that the insulator wall consisting of ceramic elements with the size equal to its thickness, soft-soldered directly to the water cooled copper substrate, was promising for the present disk generator experimental facility.

The applicability of the existing boundary layer model to the disk generator geometry was investigated. It was found that the existing model does not sufficiently describe the boundary layer phenomena on the disk generator insulator plate. Effort is being directed to develop the boundary layer model pertinent to the disk generator geometry.

The super-conducting 6 Tesla magnet was overhauled. Modifications were made to improve cryogenic thermal insulation.

Development of Insulator Walls for the Disk Generator Experimental Facility

In the last progress report we reported that there were two kinds of deterioration for the MgO ceramic insulator walls. In one case the surface

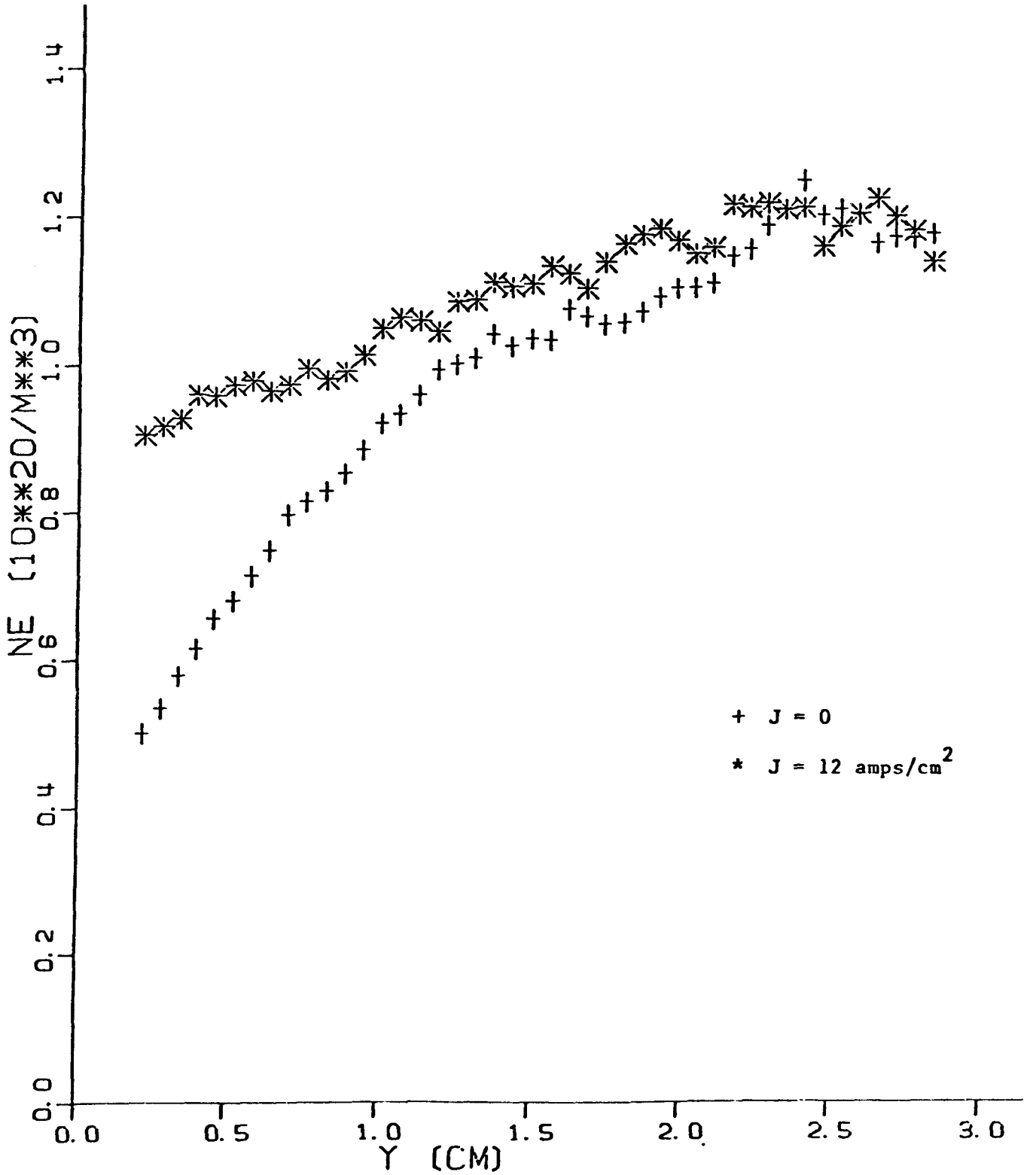

Figure 9. N_e Elevation at High Current Densities

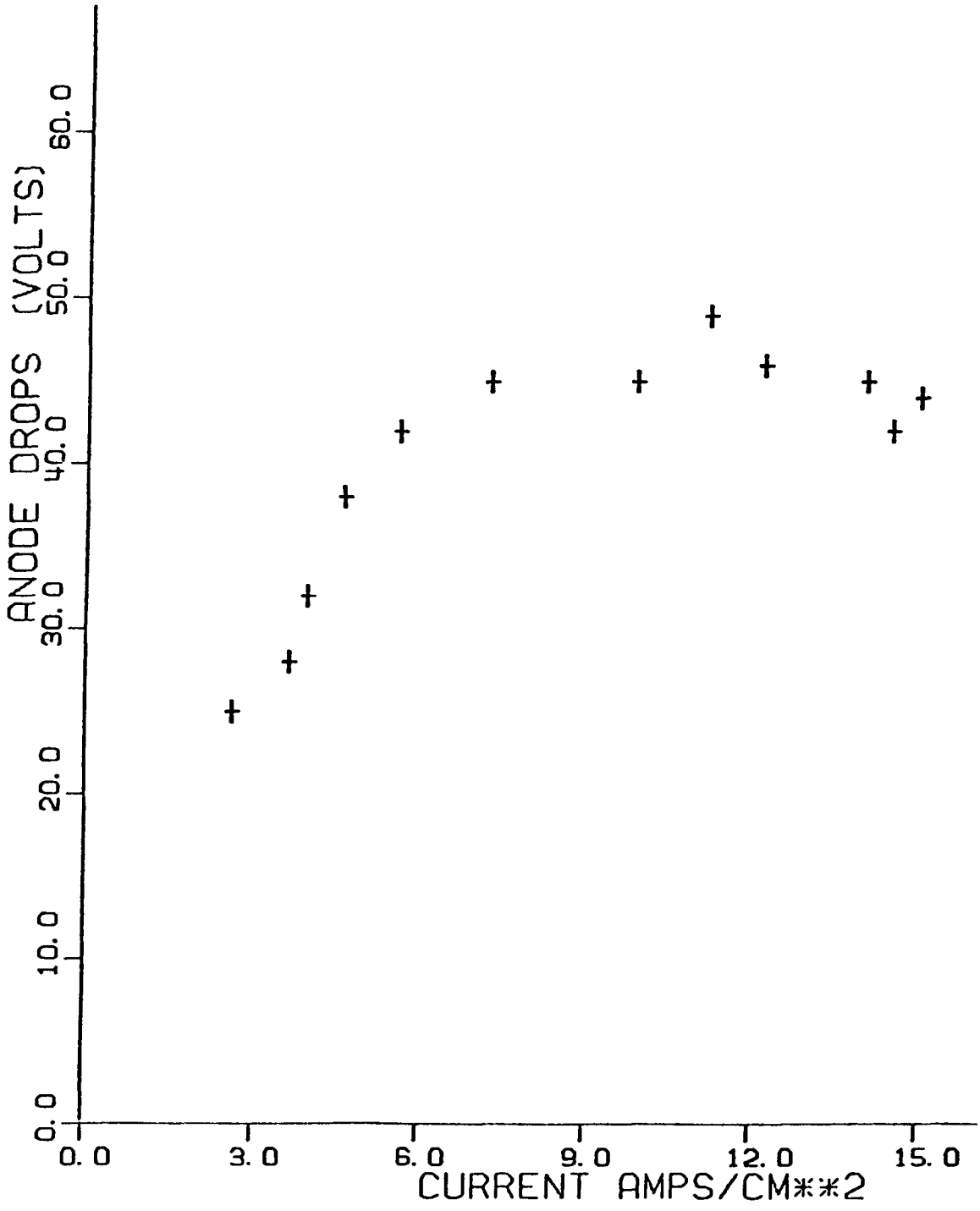

Figure 10. Anode Voltage Drops

layer of the ceramics was sheared off from the bottom layer firmly attached to the copper plate. In the other case the whole ceramic layer sheared off from the copper substrate [1]. These failures were caused by high shear stress due to the extremely high temperature gradient (~2500 K/cm). The failures were also attributed to insufficient brazing of the metalyzed ceramics to the copper substrate. The difficulty of the problem stems from the fact that thermal and electrical insulation must be achieved with a ceramic layer of less than one half inch. Though it is not possible to reduce the temperature gradient in the ceramic layer, some measures must be applied to alleviate high shear stress in order to achieve structural integrity of the insulator walls. During this quarter attempts were made to develop stress-relieving structures for the MgO ceramic insulator. One method tested was to attach the ceramics to the metal substrate with a stress-absorbing compliant layer in between. The sintered copper wire mat made of 40 μ wire (FELTMETAL by Technetics Div., Brunswick Corp.) was used as the compliant layer. With its density of 40% the thermal conductivity of the wire mat is 0.1 Watt/cm•K, about three times higher than that of the MgO ceramics. The copper coated MgO ceramics were brazed to the wire mat using Ag/Cu or Au/Cu/Pd braze material. The brazing was done in a vacuum furnace. It was observed that the wire mat tends to absorb the braze material away from the brazing interface. In some cases the braze material was totally soaked away by the wire mat. This tendency was more pronounced for Ag/Cu braze material. In order to avoid soaking, the furnace temperature was controlled to minimize the time in which the braze material was in a molten state. A disk generator insulator plate with a water cooled anode was constructed using the MgO ceramics with a wire mat compliant layer. The dimension of the MgO ceramics was the same as that of the previous insulator [2].

The insulator plate was placed at the downstream end of a linear M-2 channel during an MHD generator experiment. This arrantement was made in order to facilitate evaluation of the structure without running the full scale disk generator facility. Figure 11 shows the disk generator insulator plate with the alcohol/Oxygen/Nitrogen combustion gas impinging upon it at a 45^{o} angle. During the thermal test the surface temperature of the ceramics was monitored with an optical pyrometer. It was observed that the surface temperature of the ceramics was not uniform. This implies that the braze contact, i.e., the heat removal of that ceramic element, was not satisfactory. The poor braze contact area subsequently developed so that total separation of the braze interface occurred.

After the shutdown of the main combustion facility for laboratory modifications, thermal tests were conducted using an acetylene/oxygen or a propane/oxygen welding torch. Several different sizes of ceramics in two different groups of structures were tested. The first group consisted of the MgO ceramic with a layer of sintered copper wire mat (Figure 12a). The metalyzed MgO was brazed to the copper wire mat using Au/Cu/Pd braze alloy. A copper foil (.005") was brazed to the opposite side of the wire mat and the whole assembly was soft-soldered to the water cooled copper substrate. The second group consists of the MgO ceramic pegs that are soft-soldered directly to the water cooled substrate (Figure 12b). Care was taken to prevent the

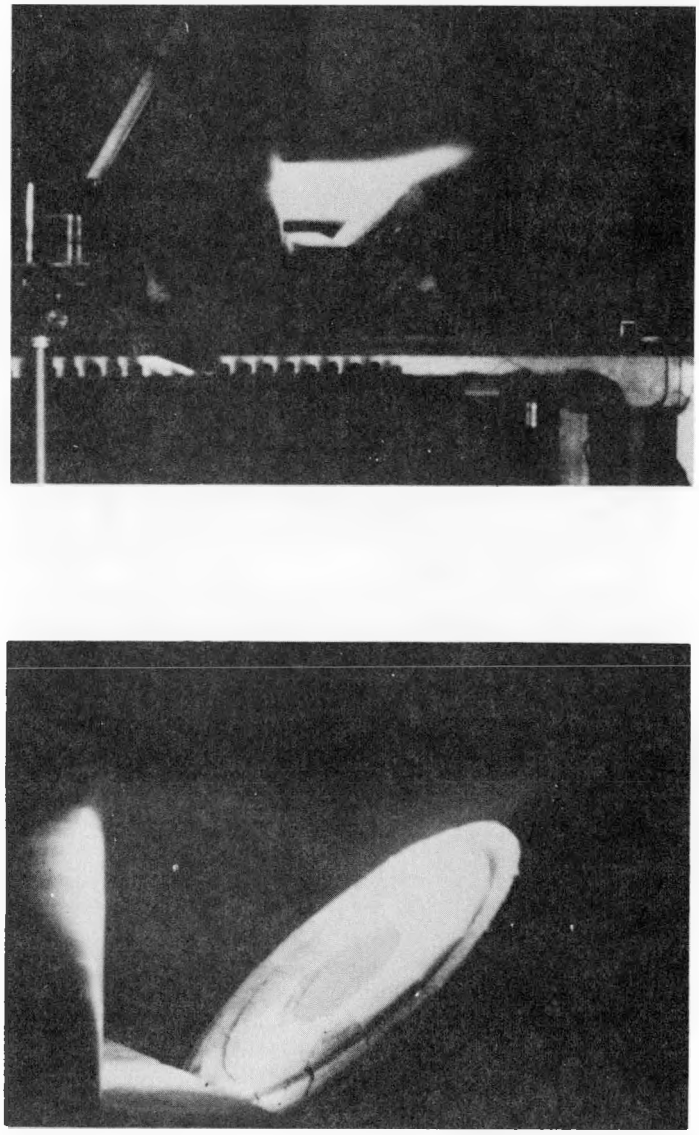

Figure 11. The disk generator insulator plate with a water cooled anode placed at the downstream end of a linear M-2 channel. The insulator plate (close-up photo, bottom) was constructed using the MgO ceramics with a copper wire mat as a complient layer.

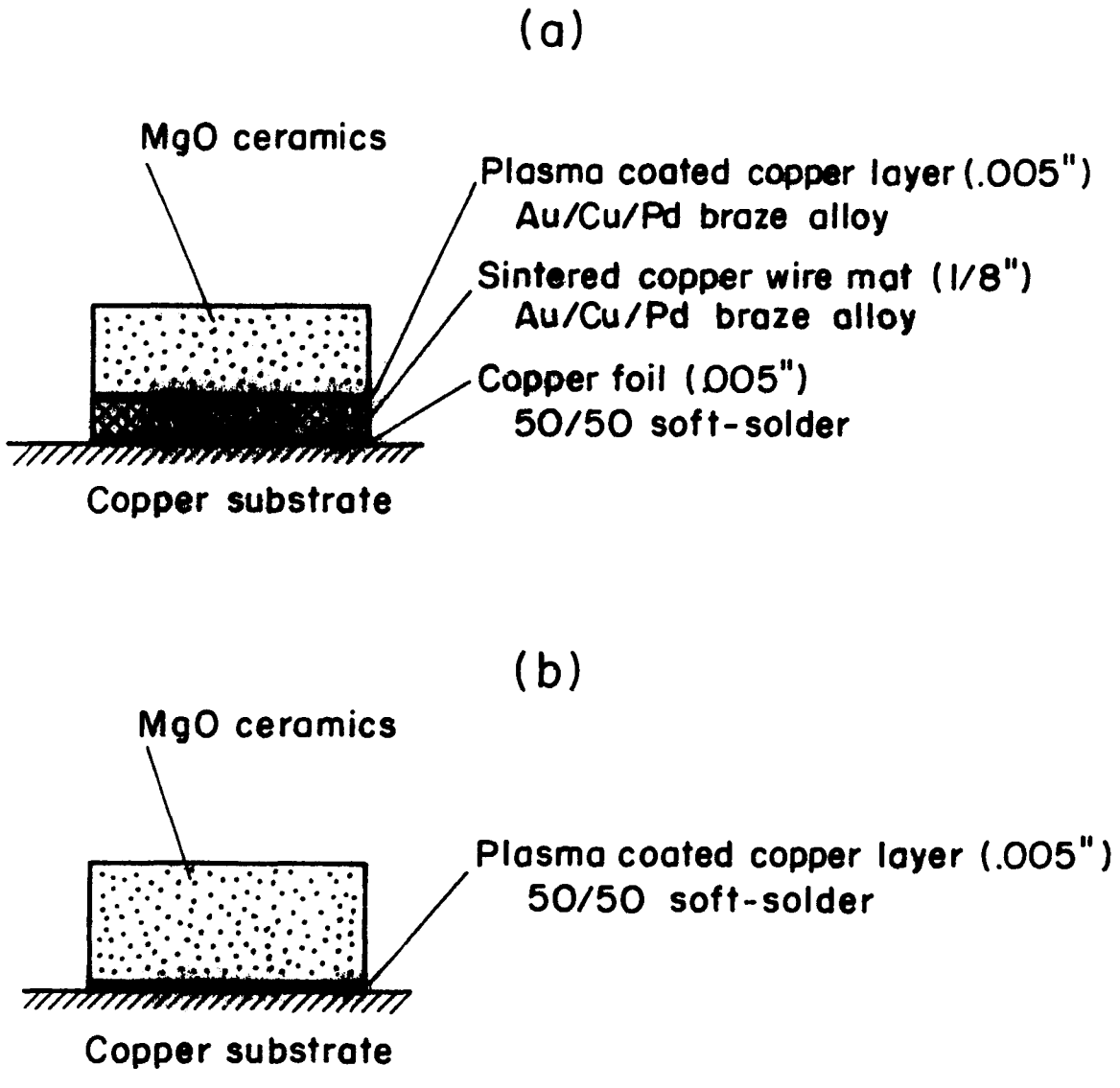

Figure 12. (a) The MgO ceramic with a layer of sintered copper wire mat, and (b) the MgO ceramic peg soft-soldered directly to the water cooled substrate.

soldering flux from penetrating to the ceramic because it was found that zinc chloride in the soldering flux deteriorates the ceramic. The dimensions of the ceramic ranged from 0.35" to 0.5" in thickness and from 0.5" to 1.0" in width.

Thermal tests were conducted for a wide range of surface temperatures and heat fluxes covering the actual disk generator experimental condition. After the thermal tests each sample was inspected. Among deteriorated samples two kinds of failures were observed. In one case the ceramic sheared off at the layer one grain size above the plasma coated copper surface. In the other case the ceramic sheared off in the center. The latter type of failure was found mostly among the samples with a compliant layer. The compliant layer does not alleviate the shear stress in the middle layer of the ceramics. The compliant layer would be effective when the temperature gradient is smaller.

In order to delineate the condition under which the MgO ceramics can be utilized, results obtained from the past thermal tests were organized according to two parameters representing the heat flux and the shear stress. In Figure 13 the ceramic samples without deterioration are marked with white symbols. The ceramic samples that deteriorated are marked with dark symbols. The horizontal bar indicates where the ceramics sheared off, i.e., either at the base or in the middle. The surface temperatures of the ceramic samples are given. The vertical axis, dT/dY, is proportional to the heat flux through the ceramics and the horizontal axis, $\Delta T \cdot L/H$, is proportional to the shear stress. (ΔT is the temperature difference across the ceramics, L and H are the size and the thickness of the ceramics, respectively.) Figure 13 indicates that for the present MgO ceramics (Magnorite by Norton Co.) the acceptable operating condition is represented by $\Delta T \cdot L/H \lesssim 2500^{o}C$. The temperature gradient, dT/dY, does not seem to have a definite effect on the integrity of the ceramic. The operating conditions of the MgO insulator wall (INS) and the electrode wall insulator (EL-INS) of UO-2 channel, Ref. 3, are within this limit. It is to be noted when the MgO ceramic is in the plastic regime this limitation may be relaxed. Since the MgO ceramics lose resiliance and become plastic above $1000^{o}C$, the ceramic element is not subject to a high thermal stress when the colder side of the ceramics layer is around $1000^{o}C$. This is the case for the two data points shown in Figure 13 for which the colder side of the ceramics layer was about $600^{o}C$, but most of the material was in the plastic range. From a purely thermal point of view it would be possible to construct an insulator wall to operate in the plastic regime. However, for the present disk generator facility it would be difficult to achieve electrical insulation under the ceramic layer. Thus it was felt appropriate to develop the insulator wall with the ceramics directly soft-soldered to the water cooled copper substrate. In this case the thermal shear stress will be alleviated by keeping the size of the ceramic element small.

An insulator wall consisting of 72 metalyzed MgO ceramics element (L=H=.5") directly soldered to the copper substrate was prepared. Thermal tests were conducted using a large propane/oxygen flame torch (900,000 btu/hr). The insulator plate was heated uniformly up to $1650^{o}C$ during a total test time of 11 minutes. None of the ceramic elements failed during the thermal test consistent with the results shown in Figure 13 as $\Delta T \cdot L/H \lesssim 1650^{o}C$ for the present case. Figure 14 shows the insulator plate after the thermal test.

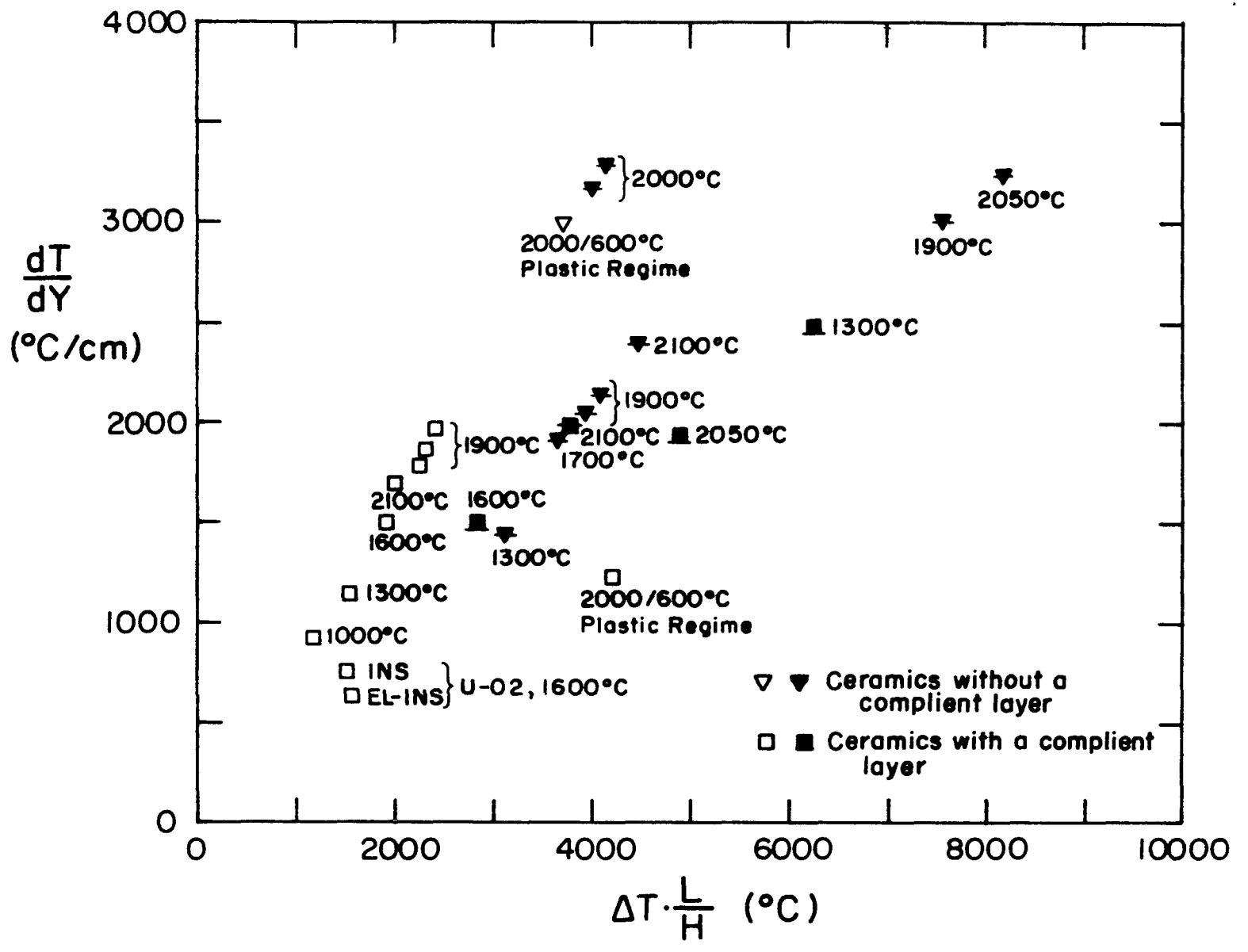

Figure 12. Structural integrity of MgO ceramics organized according to two parameters representing the heat flux and the shear stress. The vertical axes, dT/dY, is proportional to the heat flux through the ceramics and the horizontal axes, ΔT·L/H, is proportional to the shear stress. Samples without deterioration are marked with white symbols and samples that deteriorated are marked with dark symbols. The horizontal bar indicates where the ceramic sheared off, i.e., either at the base or in the middle.

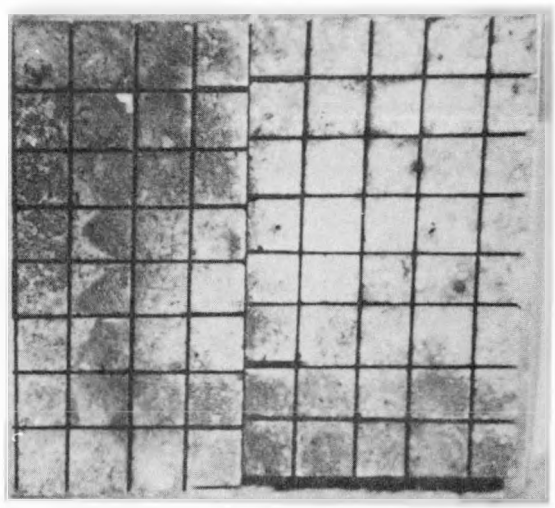

Figure 14. The insulator plate consisting of 72 metalyzed MgO ceramic elements directly soldered to the copper substrate. The insulator plate surface was heated to 1650°C for about 11 minutes.

In the next quarter the disk generator test section will be constructed by the same method and will be tested with the M-2 burner.

Boundary Layer Studies

A computer program was developed to solve the system of equations arising from the model due to Jansen [4], using characteristic dimensions of the Stanford disk generator and the properties of a combustion plasma at 2600 K and 1 atm. Comparisons were made with the friction factor as predicted by Jansen's model and that predicted by the regular momentum integral formulation for flat plate boundary layers [5]. While both correlations predicted wall friction values indicative of an entry length region, the values of Jansen were a full order of magnitude greater than the friction values predicted by the momentum thickness Reynolds number formulation.

In analyzing the values obtained for the boundary layer thickness, it was observed that the flow became fully developed about halfway down the channel. Jansen's model has a deficiency in that it apparently predicts separation when the flow becomes fully developed, so this model evidently has limited applicability in this situation.

During the next quarter further attention will be given to the momentum integral method modified to include computer determined velocity profiles.

6 Tesla Magnet

This last quarter some work was completed on the inside of the magnet prior to its being scaled up and vacuum tested. Radiation shields were designed and installed to reduce the radiation heat transfer from the room temperature sections to the cryogenic Dewars. One end cover of the iron shield was removed and then the room temperature centerbox and the 4 rectangular crosspieces were removed. Four collapsible box sections of G-10 plenolic were fabricated to support 20 layers of aluminized Mylar superinsulation, which were inserted into the rectangular openings of the crosspiece sections. Thirty layers of superinsulation were wrapped around the centerbox. All parts were degreased and reinstalled in the magnet. In the next quarter the magnet will be sealed up and the vacuum station attached, and the magnet will be tested prior to the installation of the disk channel for its first MHD test.

3.3.2 Linear Generator Program.

Work was begun this quarter to transform the general design concepts of the 6 Tesla linear channel into detailed designs. The effort was concentrated in the following areas: overall channel layout, transfer section cooling water pressure drop, transfer section construction, channel assembly procedures, interfacing of transfer sections to test section, and eliminating current leakage between MgO clad pegs.

The overall linear channel system is shown in Figure 15. As indicated, the channel will be built in three subassemblies or modules. The lead-in and

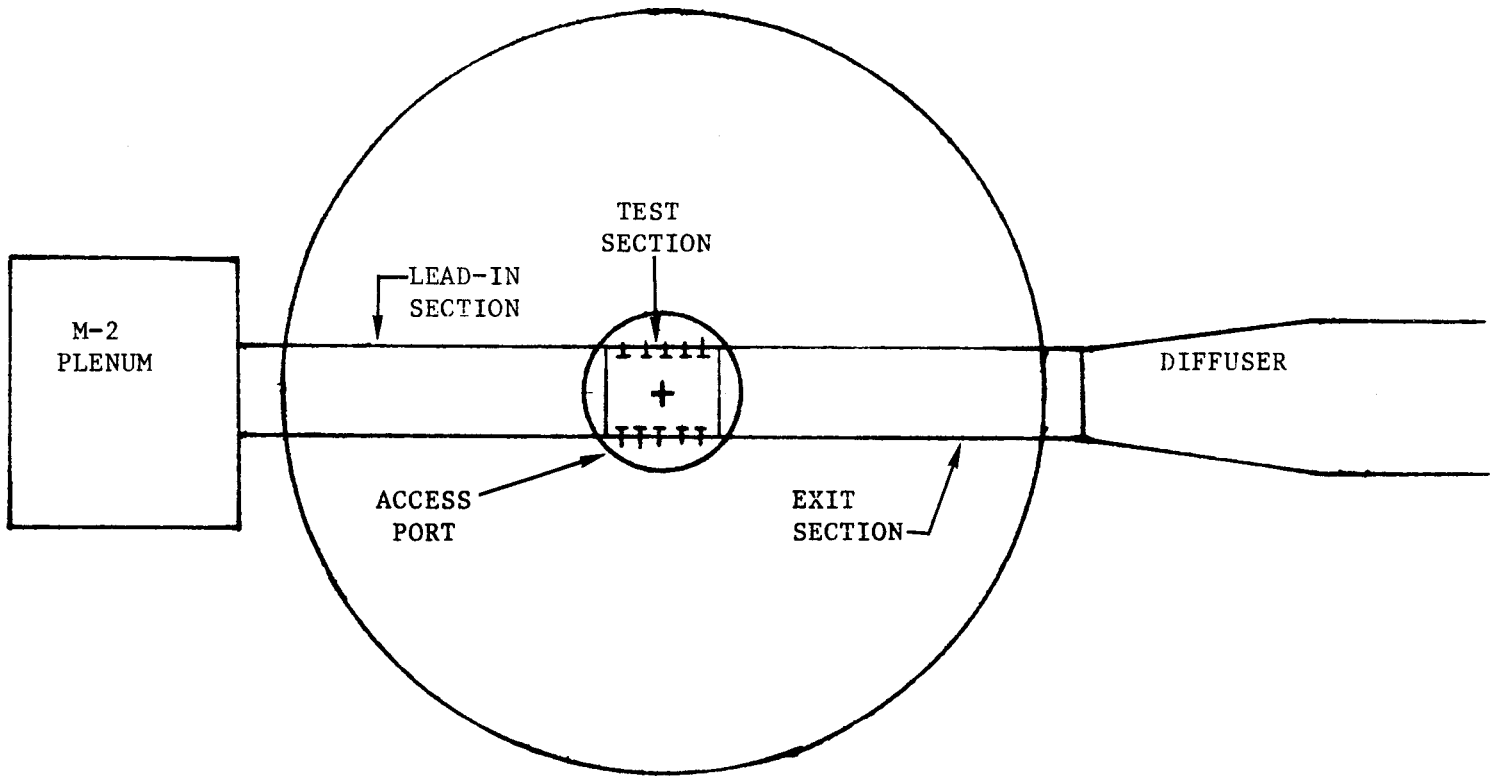

Figure 15. Linear channel in superconducting magnet.

exit sections are essentially identical in design, hereafter referred to as the transfer sections, although the critical parameters are determined by the lead-in section due to the higher heat transfer rates experienced. These insulating wall sections, described in detail in Ref. 6, fit in the 10.16 cm x 5.08 cm duct in the magnet. The third section is the test section which is located in the constant field area in the center ofthe magnet. It will be of segmented Faraday design with lanthanum chromite electrodes and peg design insulating walls. Detail design except for interface requirements has not begun on the section.

Cooling Water ΔP

In an effort to keep the magnet access port area (see Figure 14) open for instrumentation of the test section, the transfer section walls employ U-channel cooling with both the inlets and outlets outside of the magnet. This requires the cooling water to flow 79 cm in the duct over 54 cylindrical peg stems. As it is desired to keep the channel wall thin to allow maximum gas flow area, we are attempting to predict the water pressure drop accurately and keep it below 120 psi. Both model testing and computer studies are being used toward this aim.

Transfer Sections

As previously reported our hot peg wall concept (to be employed) appears sound. The problem attacked this quarter was transforming a simple pegwall concept into a channel.

The final solution is shown in Figure 16, a typical cross-section. Here the walls are held together with metal screws in the G-10 wall material, spaced 1 inch apart. With the maximum gas operating pressure of 2 atm. this results in 21 lbf on each screw, small enough for the screws to be in direct contact with the G-10. However, if in the future the channel is repeatedly dissassembled, Heli-coil inserts may be desirable and adequate material is allowed for these.

The G-10 in the corners is protected by the overlapping pegs. The channel will be sealed with RTV both at the overlapping pegs and at the G-10 corner joint. This should be adequate as a simple beam analysis indicated the maximum deflection of the G-10 between screws should be negligible.

Channel Assembly

While creating a method of constructing the channel modules, one must have in mind a method of putting the channel in the magnet. The following method has been developed. First the test section is put into place through the 17.8 cm access port in line with the rectangular ducts at the magnet's center. One transfer module is then slid in until it extends into the access port. Flanges are then attached to the transfer module's sides and it is aligned and bolted to the test section. The other transfer module is then inserted and the procedure repeated. The joint is sealed with RTV and a silicone rubber gasket. The room for the flange screws on the transfer section is available through the use of asymmetric pegs. The G-10 interface between the test and transfer sections will be a male-female arrangement.

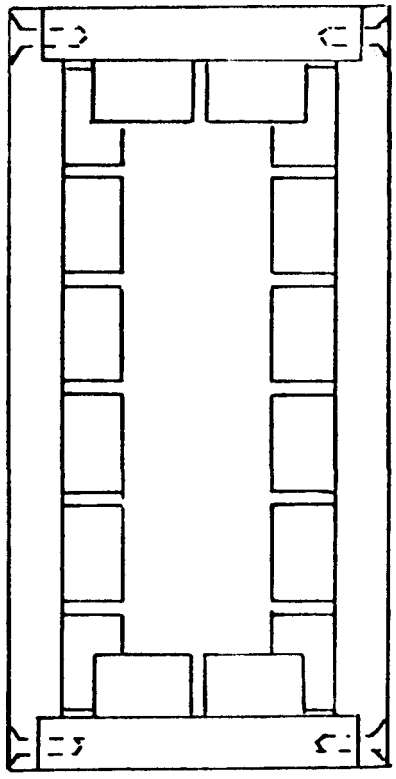

Figure 16. Transfer module cross-section.

Current Leakage

As reported last quarter unacceptable levels of current leakage were detected between our insulating wall pegs during tests. This was attributed to seed penetrating the castable ceramic in the narrow gaps between pegs and the current flowing to the copper feltmetal and peg base. To eliminate this possibility a dense insulating cement will be applied to the peg side covering the copper feltmetal and peg base. Preliminary tests indicate that a polyimide coating may be suitable. In addition .63 mm wafers of alumina will be inserted between pegs. These wafers will not extend to the top of the peg and the remaining gaps will be filled in with castable ceramic.

4.0 REFERENCES

[1] ERDA Quarterly Report for the Period July, 1976 - September, 1977, Contract No. EX 76-C-01-2341, Report No. FE-2341-4, December 1977, p. 31.

[2] ERDA Quarterly Report for the Period July, 1976 - September, 1977, Contract No. EX 76-C-01-2341, Report No. FE-2341-4, December, 1977, p. 32.

[3] Joint U. S.-U.S.S.R. Test of U.S. MHD Electrode Systems in U.S.S.R. UO-2 MHD Facility (Phase 1), Final Report, ERDA-76/154.

[4] ERDA Quarterly Report for the Period July, 1976 - September, 1977, Contract No. EX 76-C-01-2341, Report No. FE-2341-4, December, 1977, p. 36.

[5] Kays, W. M., Convective Heat and Mass Transfer, McGraw-Hill, New York (1966), p. 95.

[6] ERDA Annual Report for the Period July, 1976 - June, 1977, Contract No. EX 76-C-01-2341, Report No. FE-2341-3, July, 1977, p. 31.

☆U.S. GOVERNMENT PRINTING OFFICE: 1978-740-206/27